JACS
JOURNAL OF THE AMERICAN CHEMICAL SOCIETY
Article
pubs.acs.org/JACS

Artificial Light-Harvesting Arrays: Electronic Energy Migration and Trapping on a Sphere and between Spheres

Julien Iehl,[†] Jean-François Nierengarten,*[,†] Anthony Harriman,*[,‡] Thomas Bura,[§] and Raymond Ziessel*[,§]

[†]Laboratoire de Chimie des Matériaux Moléculaires, Université de Strasbourg et CNRS (UMR 7509), Ecole Européenne de Chimie, Polymères et Matériaux, 25 rue Becquerel, 67087 Strasbourg Cedex 02, France

[‡]Molecular Photonics Laboratory, School of Chemistry, Bedson Bldg, Newcastle University, Newcastle upon Tyne, NE1 7RU, United Kingdom

[§]Laboratoire de Chimie Moléculaire et Spectroscopies Avancées (LCOSA), Ecole Européenne de Chimie, Polymères et Matériaux, CNRS, (UMR 7515) 25 rue Becquerel, 67087 Strasbourg Cedex 02, France

Supporting Information

ABSTRACT: A sophisticated model of the natural light-harvesting antenna has been devised by decorating a C_{60} hexa-adduct with ten yellow and two blue boron dipyrromethene (Bodipy) dyes in such a way that the dyes retain their individuality and assist solubility of the fullerene. Unusually, the fullerene core is a poor electron acceptor and does not enter into light-induced electron-transfer reactions with the appended dyes, but ineffective electronic energy transfer from the excited-state dye to the C_{60} residue competes with fluorescence from the yellow dye. Intraparticle electronic energy transfer from yellow to blue dyes can be followed by steady-state and time-resolved fluorescence spectroscopy and by excitation spectra for isolated C_{60} nanoparticles dissolved in dioxane at 293 K and at 77 K. The decorated particles can be loaded into polymer films by spin coating from solution. In the dried film, efficient energy transfer occurs such that photons absorbed by the yellow dye are emitted by the blue dye. Films can also be prepared to contain C_{60} nanoparticles loaded with the yellow Bodipy dye but lacking the blue dye and, under these circumstances, electronic energy migration occurs between yellow dyes appended to the same nanoparticle and, at higher loading, to dye molecules on nearby particles. Doping these latter polymer films with the mixed-dye nanoparticle coalesces these multifarious processes in a single system. Thus, long-range energy migration occurs among yellow dyes attached to different particles before trapping at a blue dye. In this respect, the film resembles the natural photosynthetic light-harvesting complexes, albeit at much reduced efficacy. The decorated nanoparticles sensitize amorphous silicon photocells.

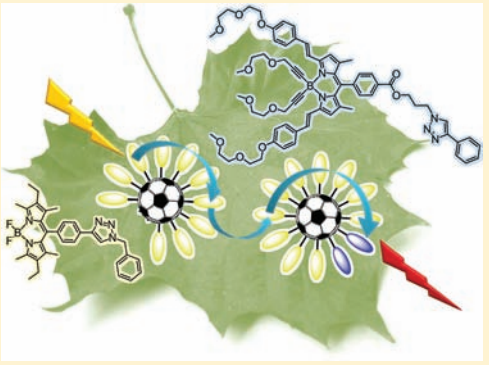

INTRODUCTION

Photosynthetic organisms are exquisitely tailored so as to capture incident sunlight with high efficacy[1] and transmit the transient excitation energy to a reaction center where chemical reactions are initiated.[2] The energy-transfer mechanism is often described by semiclassical models that invoke 'hopping' of the wave packet along discrete energy levels and over considerable distances set in three-dimensional space.[3] These energy levels combine to form a large peripheral light-harvesting antenna coupled to individual reaction centers. Many attempts have been made to duplicate the essential features of the natural process, ignoring elaborate events such as self-repair and quantum coherence,[4] and great progress has been made in understanding the underlying energy-transfer steps. Mostly, these bioinspired molecular systems have been studied as standalone entities in one- or two-dimensions, although some consideration has been given to the design of three-dimensional arrays, such as dendrimers,[5] polymers,[6] organo-gels,[7] and carbon-based nanometric networks,[8] and to the use of quantum dots dispersed in a polymer film.[9] The next major challenge in this field relates to identifying molecular arrays, themselves being capable of effective energy transfer around the cluster, that readily enter into longer range energy transfer to nearby arrays. In this manner, the exciton can migrate over unusually large distances, as in natural photon collectors, until trapped at a specific site. This has not been done in any artificial system, but the photon collector reported here goes some way to meeting this ambitious goal. In developing this new molecular architecture, it should be stressed that some severe synthetic challenges had to be overcome, most notably by the need to generate asymmetrical structures with a high density of chromophores retaining spatial integrity. In particular, we

Received: July 23, 2011
Published: December 8, 2011

 © 2011 American Chemical Society dx.doi.org/10.1021/ja206894z | J. Am. Chem.Soc. 2012, 134, 988–998

sought to avoid the random distribution of dyes around a central core.

The first requisite for next-generation artificial light-harvesting arrays is a robust, synthetically amenable scaffold that readily facilitates 3-D arrangements of complementary chromophores. Our initial attention focused on C_{60} as a compact, spherical building block.[10] The essential functionality is provided by a mixed hexa-adduct of C_{60} bearing ten azide groups and two TMS-protected alkyne units, thereby allowing the successive grafting of ten terminal alkyne and two azide modules via consecutive click reactions.[11] This strategy is appealing because, in addition to providing a suitable route by which to decorate the outer surface of the sphere with an organic dye, it lends itself readily to the isolation of asymmetric structures where two disparate dyes can be loaded onto the same nanoparticle. In principle, the fullerene core might also play an active role in the excited state deactivation of the resulting ensemble.[12] Compared to the corresponding mono- and bis-adducts, however, fullerene hexa-adducts are poor electron acceptors and exhibit only very weak absorption in the visible region.[13] A further, and indeed critical, advantage of these particular fullerenes relates to their relatively high solubility and ease of dissolution in organic solvents, especially after decoration with a peripheral layer of dye. This facilitates reaching high concentrations of reagents without serious problems from aggregation, a situation impossible to realize with either conventional fullerenes or planar polycyclic dyes. Boron dipyrromethene (Bodipy) dyes are ideally suited for use as the organic emitters because they are easily functionalized, highly fluorescent, and robust and eagerly enter into energy-transfer reactions with suitable partners.[14,15] To provide a gradient of energy levels, we opted to use the Bodipy dyes $\mathbf{Y_1}$ and $\mathbf{B_1}$ (Figure 1), which are equipped with contrasting conjugation lengths and hence inequivalent optical properties (namely, yellow and blue absorbers, respectively).

Light-induced electron transfer from the excited-state of a dye to the hexa-substituted C_{60} core is thermodynamically unfavorable and spectral overlap between absorption by the fullerene and emission from the dye is low, thus minimizing singlet−singlet energy transfer to the C_{60} unit (see Supporting Information).[16] Furthermore, triplet−triplet energy transfer is less important in this system since the Bodipy dyes have poor spin−orbital coupling properties and resist intersystem crossing. Consequently, it might be anticipated that the C_{60} hexa-adduct will be content to operate as a passive scaffold without intercepting light-driven events involving the outer coating of dye molecules. This is a critical feature of these prototypic artificial photon collectors. The hexa-adduct also facilitates the construction of 3D structures such that large intercommunicating networks might become possible by linking together a string of decorated nanoparticles in much the same way that natural analogues function to direct excitons over surprisingly large distances. To do this effectively, a functional solid-state device needs to be equipped with some degree of coherence, this latter point being a massive challenge in terms of supramolecular chemistry. Over the past four decades, considerable research has been devoted to the construction of plastic solar concentrators whereby a fluorescent dye is embedded in the polymeric matrix. Fluorescence from the dye is retained within the plastic sheet by way of internal reflectance and transmitted to the edges, where an expensive solar cell is located. The combination of transparent plastic and embedded dye work together to form a cheap light guide. The threshold wavelength for output from the dye is controlled by the emission profile while the collection efficiency is improved by using a cocktail of dyes able to enter into electronic energy-transfer processes. Such devices are commercially available but suffer from problems of self-absorption and, like many organic molecules, poor photostability. A critical aspect of our prototype is that it overcomes the self-absorption problem while using extremely stable dyes. An important point to bear in mind is that solar fuel production demands the ability to drive multielectron reactions and, in turn, this needs an adequate supply of photons at the reaction site. A solar concentrator, therefore, will be mandatory for many photochemical systems aimed at artificial photosynthesis.

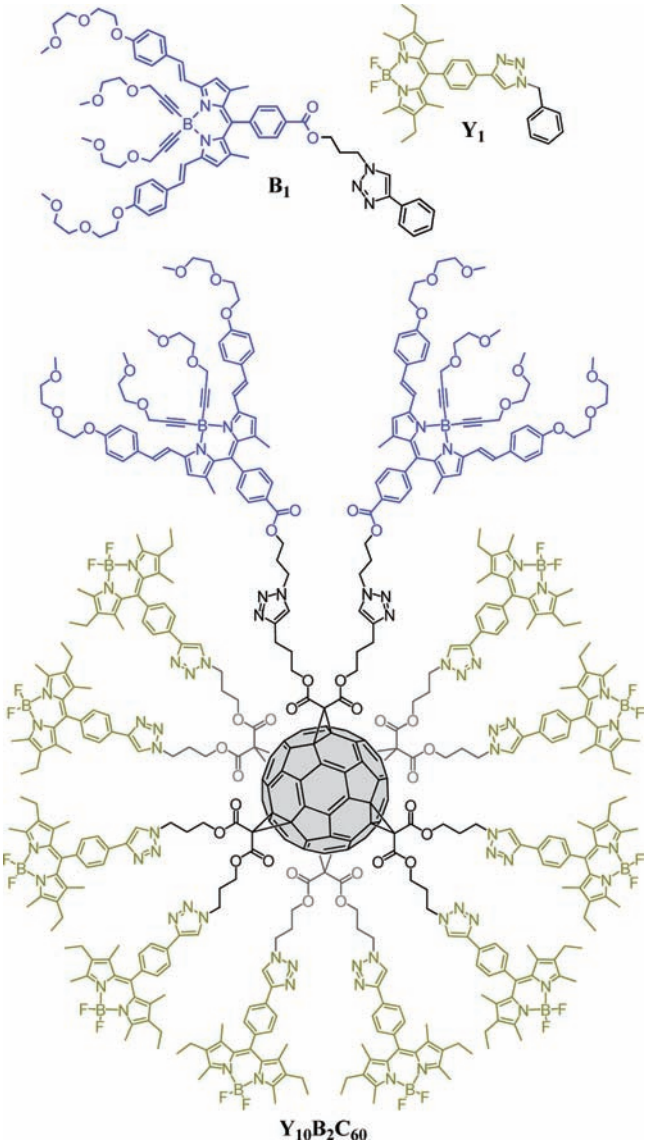

Figure 1. Top: Model Bodipy compounds $\mathbf{Y_1}$ (yellow) and $\mathbf{B_1}$ (blue) bearing the triazole ring produced by click chemistry and used throughout this work as control dyes. Bottom: C_{60} hexa-adduct $\mathbf{Y_{10}B_2C_{60}}$ decorated with yellow and blue Bodipy-based dyes.

RESULTS AND DISUSSION

Electronic Energy Transfer on Isolated Nanoparticles.

The synthesis of the Bodipy-C_{60} hexa-adduct $\mathbf{Y_{10}B_2C_{60}}$ and those of the corresponding model compounds $\mathbf{Ph_{10}C_{60}}$, $\mathbf{Y_{10}C_{60}}$,

dx.doi.org/10.1021/ja206894z | J. Am. Chem.Soc. 2012, 134, 988−998

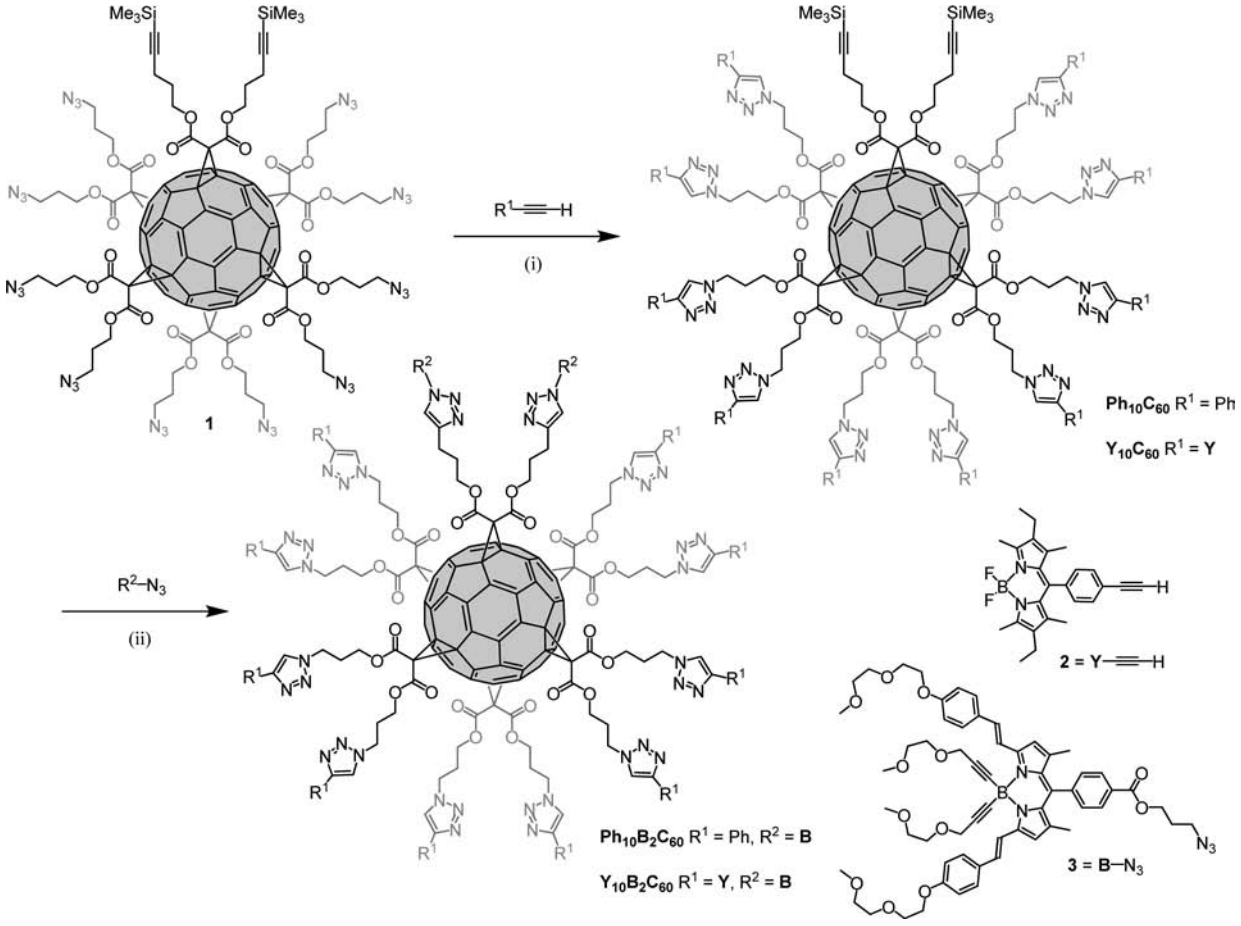

Figure 2. Reagents and conditions: (i) sodium ascorbate, $CuSO_4{\cdot}5H_2O$, CH_2Cl_2/H_2O (1/1), 25 °C [from **2**: $\mathbf{Y_{10}C_{60}}$ (61%), from phenylacetylene: $\mathbf{Ph_{10}C_{60}}$ (78%)]; (ii) **3**, TBAF, sodium ascorbate, $CuSO_4{\cdot}5H_2O$, CH_2Cl_2/H_2O (1/1), 25 °C [from $\mathbf{Y_{10}C_{60}}$: $\mathbf{Y_{10}B_2C_{60}}$ (43%), from $\mathbf{Ph_{10}C_{60}}$: $\mathbf{Ph_{10}B_2C_{60}}$ (81%)].

and $\mathbf{Ph_{10}B_2C_{60}}$ are outlined in Figure 2. Reaction of precursor **1** with a slight excess of terminal alkyne **2** (11 equiv) in the presence of $CuSO_4{\cdot}5H_2O$ (0.1 equiv) and sodium ascorbate (0.3 equiv) in CH_2Cl_2/H_2O gave $\mathbf{Y_{10}C_{60}}$ in 64% yield. In contrast, $\mathbf{Ph_{10}C_{60}}$ was obtained by treatment of **1** with phenylacetylene. Importantly, the two TMS-protected alkyne units remain unreactive under these conditions. In both cases, IR spectroscopy confirmed the absence of azide ($\nu_{N=N}$ = 2092 cm^{-1}) residues from the isolated products. Finally, treatment of $\mathbf{Ph_{10}C_{60}}$ and $\mathbf{Y_{10}C_{60}}$ with **3** in the presence of tetrabutylammonium fluoride (TBAF), $CuSO_4{\cdot}5H_2O$, and sodium ascorbate in CH_2Cl_2/H_2O gave the target [5:1] fullerene hexa-adducts $\mathbf{Ph_{10}B_2C_{60}}$ and $\mathbf{Y_{10}B_2C_{60}}$, respectively. The structures of both compounds were confirmed by MALDI-TOF mass spectrometry and their IR and ^1H and ^{13}C NMR spectra. As is often observed for mixed fullerene hexa-adducts,[11,17] the ^1H NMR spectra show slight broadening of the signals. Indeed, the overall C_{2v} symmetry of these loaded nanoparticles leads to complicated spectra because the ten **Y** or **Ph** units are magnetically inequivalent. However, close inspection of the ^1H NMR spectra reveals that the two different kinds of malonate addends are in the expected 5:1 ratio for both $\mathbf{Ph_{10}B_2C_{60}}$ and $\mathbf{Y_{10}B_2C_{60}}$.

To ensure that the C_{60} core will not function as an electron acceptor and thereby interfere with electronic energy transfer (EET) between the Bodipy dyes, cyclic voltammograms were recorded for $\mathbf{Y_{10}B_2C_{60}}$, $\mathbf{Y_{10}C_{60}}$, and $\mathbf{Ph_{10}B_2C_{60}}$ in CH_2Cl_2 containing background electrolyte and referenced to ferrocene ($E_{1/2}$ = 0.38 V vs SCE) as an internal standard (Figure 3). Peak assignment was made by way of adding an equimolar amount of

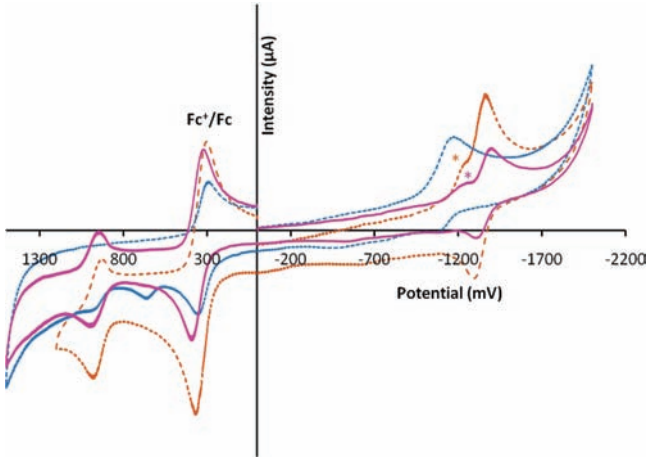

Figure 3. Cyclic voltammograms of (---) $\mathbf{Y_{10}B_2C_{60}}$, (···) $\mathbf{Y_{10}C_{60}}$, and (—) $\mathbf{Ph_{10}B_2C_{60}}$ in CH_2Cl_2 containing 0.1 M tetra-*n*-butylammonium hexafluorophosphate at 20 °C; scan rate 200 mV s^{-1}. All peaks were calibrated against ferrocene (Fc^+/Fc) at $E_{1/2}$ = 0.38 V vs SCE. Peaks marked with an asterisk correspond to the reduction of the C_{60} subunits.

dx.doi.org/10.1021/ja206894z | J. Am. Chem.Soc. 2012, 134, 988–998

either **Y** or **B**. No peaks could be observed on oxidative scans performed with the naked C_{60} adducts (Table 1), but peaks are clearly evident when the outer surface is coated with a Bodipy dye. Thus, the first reversible peak corresponds to a half-wave potential, $E_{1/2}$, of 0.99 V vs SCE for $\mathbf{Y_1}$ and 0.69 V vs SCE for $\mathbf{B_1}$ and is ascribed to formation of the Bodipy π-radical cation.[18] The second and third peaks, these being electrochemically irreversible, seen for systems containing $\mathbf{B_1}$ are due to oxidation of the styryl side arms.[19] A series of peaks are seen on reductive scans (Table 1). Reversible, one-electron reduction steps are apparent for the two Bodipy dyes, with $\mathbf{B_1}$ being somewhat easier to reduce to the π-radical anion. For $\mathbf{Ph_{10}C_{60}}$, an irreversible reductive wave is found with a peak potential of ca. −1.2 V vs SCE that can be assigned to reduction of the C_{60} residue. For $\mathbf{Y_{10}C_{60}}$, it is possible to resolve reduction of both the C_{60} core and the peripheral dyes, with the latter being more easily reduced. With $\mathbf{Ph_{10}B_2C_{60}}$, however, reduction of the C_{60} unit overlaps that of the Bodipy residue (Table 1). On the basis of these various electrochemical results, it is possible to eliminate the likelihood of light-induced electron transfer occurring in weakly polar media (see Supporting Information for further details).

Table 1. Electrochemical Data for the Hybrid C_{60}-Multidye Clusters and Appropriate Reference Compounds[a]

	E^0(ox, soln) (V), ΔE (mV)	E^0(red, soln) (V), ΔE (mV)
$\mathbf{Y_1}$	+0.99 (60)	−1.31 (60)
$\mathbf{B_1}$	+0.69 (60); +1.11 (irr); +1.27 (irr)	−1.13 (80); −1.78 (irr)
$\mathbf{Ph_{10}C_{60}}$	–	−1.24 (irr)
$\mathbf{Y_{10}C_{60}}$	+1.00 (60)	−1.22 (irr), −1.28 (60)
$\mathbf{Ph_{10}B_2C_{60}}$	+0.72 (irr) ; +1.05 (irr)	−1.17 (irr)[b]
$\mathbf{Y_{10}B_2C_{60}}$	+1.00 (60)	−1.22 (60), −1.33 (70)

[a]Potentials determined by cyclic voltammetry in deoxygenated CH_2Cl_2 solution, containing 0.1 M $TBAPF_6$, at a solute concentration of ca. 1.5 mM and at rt. Potentials were standardized versus ferrocene (Fc) as internal reference and converted to the SCE scale assuming that $E_{1/2}$ (Fc/Fc$^+$) = +0.38 V (ΔE_p = 60 mV) vs SCE. Error in half-wave potentials is ±15 mV; for irreversible processes, the peak potentials (E_{ap}) or (E_{cp}) are quoted. [b]Broad peak due to overlapping of several redox processes.

The photophysical properties of the two isolated Bodipy dyes, $\mathbf{Y_1}$ and $\mathbf{B_1}$, are similar to those reported for related dyes.[20,21] It is notable that the triazole linker has no obvious effect on these properties and, in particular, both dyes remain strongly fluorescent in fluid solution and after dispersal in a poly(methylmethacrylate) (PMMA) film. For each of these reference compounds in dioxane solution, the fluorescence quantum yield (Φ_F), excited-singlet state lifetime (τ_S), radiative rate constant (k_{RAD}), absorption maximum (λ_{ABS}), and fluorescence maximum (λ_{FLU}) are as expected on the basis of earlier work[20,21] with related materials (Table 2). Electronic energy transfer is expected to occur from $\mathbf{Y_1}$ to $\mathbf{B_1}$, driven by the energy gap of 3640 cm^{-1}. Moreover, there is a modest spectral overlap integral[22] (J_{DA}) for energy transfer, which when used in conjunction with the measured photophysical and spectroscopic properties translates to a Förster critical distance[23] (R_{CD}) of ca. 25 Å (see Supporting Information for methodology). It is also pertinent to consider energy migration between identical $\mathbf{Y_1}$ molecules. Here, J_{DA} is comparable to that measured for energy transfer from yellow to blue dye, because of the small Stokes shift, while the computed R_{CD} is conducive to efficient photon hopping between $\mathbf{Y_1}$ molecules at high local concentrations. These various values are collated in Table 2. A similar situation is found for energy migration between $\mathbf{B_1}$ molecules in dioxane solution.

Turning attention now to the C_{60}-appended dyes, we note that fluorescence is readily apparent for both $\mathbf{Y_{10}C_{60}}$ and $\mathbf{Ph_{10}B_2C_{60}}$ in dioxane solution and when loaded into PMMA films. In fluid solution, the recorded photophysical data are indicative of inefficient electronic energy transfer from the Bodipy dye to the C_{60} core; the latter is very weakly fluorescent,[24] and there is a low spectral overlap integral. The net result is that τ_S for the appended dye is somewhat reduced, and there is a small effect on the computed R_{CD} values (Table 2). This effect, which is independent of concentration and temperature, is unfortunate but far from catastrophic; the rate constant for energy transfer (k_{EET}) from yellow dye to C_{60} core, determined by comparison of emission lifetimes for the isolated yellow dye and $\mathbf{Y_{10}C_{60}}$, is 5.6×10^8 s^{-1}. Absorption spectroscopy does not indicate aggregation of either dye or fullerene over a 100-fold variation in concentration while the fluorescence quantum yield is also independent of concentration in the range 1−40 μM. Dynamic light-scattering experiments[25] carried out as a function of concentration in dioxane confirm that the C_{60} nanoparticles act independently and do not accrete into larger structures over several days standing in the dark. In this respect, the decorated nanoparticles behave differently from conventional fullerenes in solution;[26] it is also notable that the decorated C_{60} nanoparticles dissolve readily without sonication. Similar experiments made with $\mathbf{Ph_{10}B_2C_{60}}$ show much slower energy transfer to the fullerene ($k_{EET} = 7.5 \times 10^7$ s^{-1}) because of significantly weaker spectral overlap between blue dye and C_{60} compared to that found for C_{60} and the yellow dye. An absorption spectrum recorded for an equimolar mixture of these two nanoparticles

Table 2. Photophysical Properties Recorded for the Bodipy-Based Dyes in Dioxane Solution

dye	λ_{ABS}/nm	λ_{FLU}/nm	Φ_F	τ_S/ns	$k_{RAD}/10^8$ s^{-1}	process	J_{DA}/cm	R_{CD}/Å
$\mathbf{Y_1}$	522	540	0.75[c]	4.8	1.6	Y→B	0.000075	23.7
$\mathbf{Y_1}$						Y→Y	0.000086	27.3
$\mathbf{B_1}$	646	665	0.56[d]	4.2	1.4	B→B	0.000353	26.7
$\mathbf{Y_{10}C_{60}}$	525	545	0.17[c]	1.3	1.3	Y→Y	0.000090	23.5
$\mathbf{Ph_{10}B_2C_{60}}$	647	665	0.44[d]	3.2	1.4	B→B	0.000330	27.4
$\mathbf{Y_{10}B_2C_{60}}$[a]	648	665	0.46	3.4	1.4	B→B	0.000325	27.4
$\mathbf{Y_{10}B_2C_{60}}$[b]	525	545	0.026	0.29[e]	NA	Y→B	0.000078	20.3

[a]Refers to the blue dye. [b]Refers to the yellow dye. [c]Excitation at 490 nm. [d]Excitation wavelength 610 nm. [e]Refers to the mean lifetime extracted by integration of stretched exponential decay curves.

dx.doi.org/10.1021/ja206894z | J. Am. Chem.Soc. 2012, 134, 988−998

shows that the yellow dye can be selectively illuminated at ca. 495 nm, where the blue dye absorbs 5% of incident photons, while the latter can be illuminated exclusively at wavelengths longer than 550 nm.

Moving now to the hybrid cluster, $\mathbf{Y_{10}B_2C_{60}}$, we note first that the absorption spectrum across the visible region is indistinguishable from that of a 1:1 molar mixture of $\mathbf{Y_{10}C_{60}}$ and $\mathbf{Ph_{10}B_2C_{60}}$ in dioxane solution, at all accessible concentrations. This indicates that the various dyes do not aggregate on the C_{60} surface. Fluorescence from both yellow and blue dyes can be recognized easily for the hybrid. Illumination at 610 nm gives rise to emission solely from the blue dye (Figure 4), and the derived photophysical properties are closely comparable to those recorded for $\mathbf{Ph_{10}B_2C_{60}}$ in

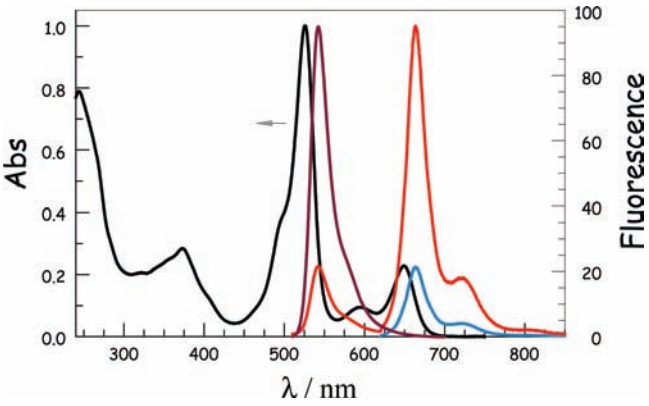

Figure 4. Absorption (black curve, arrowed) and fluorescence (red curve, λ_{EX} = 495 nm) spectra recorded for $\mathbf{Y_{10}B_2C_{60}}$ in dioxane. Superimposed are fluorescence spectra for the yellow (plum curve) and blue (blue curve) dyes, each being normalized to the corresponding absorption band maximum.

dioxane solution (Table 2). There is no additional effect due to the presence of an appended yellow dye. Under the same conditions, illumination of the yellow dye at 490 nm results in weak fluorescence from that emitter together with much stronger fluorescence from the blue dye (Figure 4). Comparison with the equimolar mixture indicates that emission from the yellow dye in the hybrid cluster is quenched by about 85%, taken from the respective steady-state fluorescence measurements, and there is a concomitant increase in fluorescence from the blue dye. Thus, efficient EET occurs from yellow to blue dyes on the C_{60} surface; a fact supported by comparison of excitation and absorption spectra. In dioxane, the probability (P_{EET}) of intraparticle energy transfer, measured by integration of the respective fluorescence signals for yellow and blue dyes compared to the mixture, is independent of the concentration of $\mathbf{Y_{10}B_2C_{60}}$ over a wide range but increases slightly with increasing temperature. A closely comparable P_{EET} value (P_{EET} = 82%) is obtained by matching excitation and absorption spectra recorded under identical conditions. On freezing the solvent to 77 K, P_{EET} falls to a lower limit of about 50%. Under these latter conditions, excitation spectra confirm that quenching of yellow emission is due to intraparticle EET while strong fluorescence is observed from the blue dye. As such, there is no suggestion that Bodipy dyes self-associate under these conditions. In particular, the emission spectra show no contribution from an emissive dimer at 77K.[27]

Time-resolved emission spectral studies carried out with $\mathbf{Y_{10}B_2C_{60}}$ and $\mathbf{Ph_{10}B_2C_{60}}$ in dioxane show that the blue absorber retains a fluorescence lifetime of 3.3 ± 0.2 ns in both cases (Table 2). In contrast, nonexponential decay kinetics appear for fluorescence isolated from the yellow dye present as part of $\mathbf{Y_{10}B_2C_{60}}$ (Figure 5). After deconvolution of the instrumental response function, emission from the yellow dye can be well described by way of the stretched-exponential

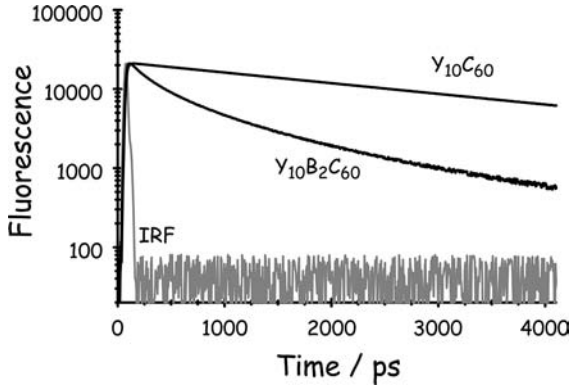

Figure 5. Time-resolved fluorescence decay curves recorded for the yellow dye appended to the nanoparticle. Excitation is directly into the yellow dye at 505 nm, and detection is made at 550 nm. Apart from the instrumental response function (IRF), decays are shown for $\mathbf{Y_{10}C_{60}}$ and $\mathbf{Y_{10}B_2C_{60}}$ for comparative purposes.

function[28] as expressed in eq 1. Here, the emission intensity (I_F) recorded as a function of time (t) is considered in terms of a scaling factor A, a time constant τ_K that is characteristic of the trapping process, and a stretching exponent β that is representative of the heterogeneity of the deactivation process. Integration[29] of this function, according to eq 2 where Γ is the gamma function, gives rise to the mean relaxation time, $\langle\tau\rangle$, for the excited state resident on the yellow absorber. The latter parameter derived following preferential excitation into the yellow dye, which refers to a combination of trapping by way of EET to the blue dye and energy migration among yellow dyes, is 290 ± 20 ps. This allows a further estimate of P_{EET} (= 78%) by comparison with the excited-state lifetime for the yellow dye present in $\mathbf{Y_{10}C_{60}}$.

$$I_F(t) = Ae^{-(t/\tau_K)^\beta} \quad (1)$$

$$\langle\tau\rangle = \int_0^\infty dt e^{-(t/\tau_K)^\beta} = \frac{\tau_K}{\beta}\Gamma\left(\frac{1}{\beta}\right) \quad (2)$$

Data analysis can be continued by way of fitting data collected at different emission wavelengths and over various concentrations to eq 1 so as to provide realistic estimates for the time constant and stretching exponent. Nonlinear, least-squares fitting procedures lead to consistent values of τ_K = 120 ps and β = 0.44 (Figure 6); recall that a single-exponential decay curve is recovered for β = 1. These parameters have to be treated with caution because the analysis is somewhat correlated but the derived τ_K value seems entirely in line with EET from yellow to blue dyes appended to the same nanoparticle (see below). The β value obtained from these fits is indicative of the competitiveness of energy migration among the yellow dyes with respect to EET to a blue dye. A value of β = 0.44 implies that energy migration is the more favorable route. Measurements made in dioxane solution over a small temperature range show that $\langle\tau\rangle$ decreases progressively

dx.doi.org/10.1021/ja206894z | J. Am. Chem.Soc. 2012, 134, 988–998

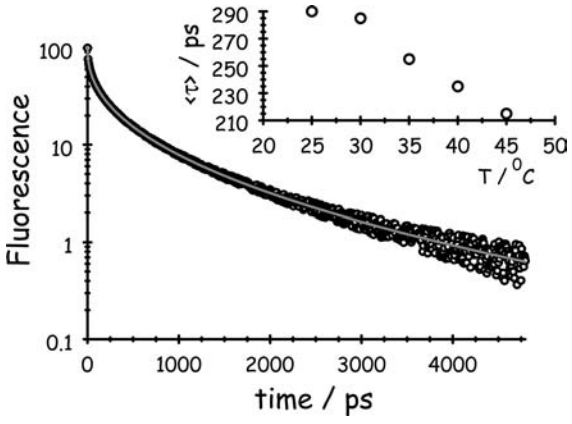

Figure 6. Example of a fit to the time-resolved fluorescence decay curve recorded for the yellow dye present in $Y_{10}B_2C_{60}$ to a stretched exponential with τ_K = 120 ps and β = 0.44. The insert shows how the mean relaxation time, $\langle\tau\rangle$ obtained from integration of the decay curve, depends on temperature.

with increasing temperature in line with expectations raised on the basis of diffusional motion of dyes appended to the C_{60} sphere (Figure 6 insert).

We suppose that an excited-singlet state of the yellow dye when bound to the C_{60} core can undergo three distinct energy-transfer steps, namely, transfer to C_{60}, to a blue dye on the same particle, or to a nearby yellow dye (Scheme 1). The first process is slow, accounting for <10% of the initial excited-state population, while analysis of the spectroscopic data in terms of Förster theory[30] indicates that the rate of EET to a yellow dye will be ca. 2.4-fold faster than transfer to a blue dye held at the same separation distance. Energy migration between yellow dye molecules decorating the C_{60} particle, therefore, will compete favorably with irreversible EET to a blue dye. The topology of the loaded C_{60} nanoparticle is dynamic on the time scale of energy transfer,[31] making it impossible to estimate separation distances with any real certainty.[23] Furthermore, according to the synthetic protocol employed, yellow and blue dyes are attached in pairs corresponding to a crude octahedral arrangement. This positioning has four yellow pairs in reasonably close proximity to a blue pair, but the remaining yellow pair is distal from the blue trap. The tether restrains the topology to such an extent that no dye can be more than ca. 25 Å from a dye molecule of a different pair. This is near to the critical distances but, in most cases, dye molecules will be closer. As such, it is not unreasonable to expect fast energy migration and trapping on the particle (Scheme 1).

We have considered the EET processes expected to occur on a decorated nanoparticle as follows: Molecular modeling[32] of an isolated nanoparticle equipped with only one pair of yellow dyes shows that the two Bodipy units adopt an average conformation that corresponds to a B−B separation of ca. 19.5 Å (see Supporting Information), although the structure is dynamic. A similar study made for an isolated pair of blue dyes gives an average B−B separation of 21.8 Å. In the case of the yellow dyes, adding the remaining four pairs causes the original pair of fluorophores to move further apart so that the notion of having five pairs of dyes disappears in favor of ten spatially isolated yellow dyes decorating the surface of the sphere. The average separation remains reasonably consistent because of spatial crowding, the blocking effects of the alkyl groups attached to the dipyrrin backbone, and the relatively short

Scheme 1. Pictorial Illustration of the Intraparticle EET Steps Proposed for Selective Excitation of a Yellow Dye on a $Y_{10}B_2C_{60}$-Decorated Nanoparticle Maintained in Isolation[a]

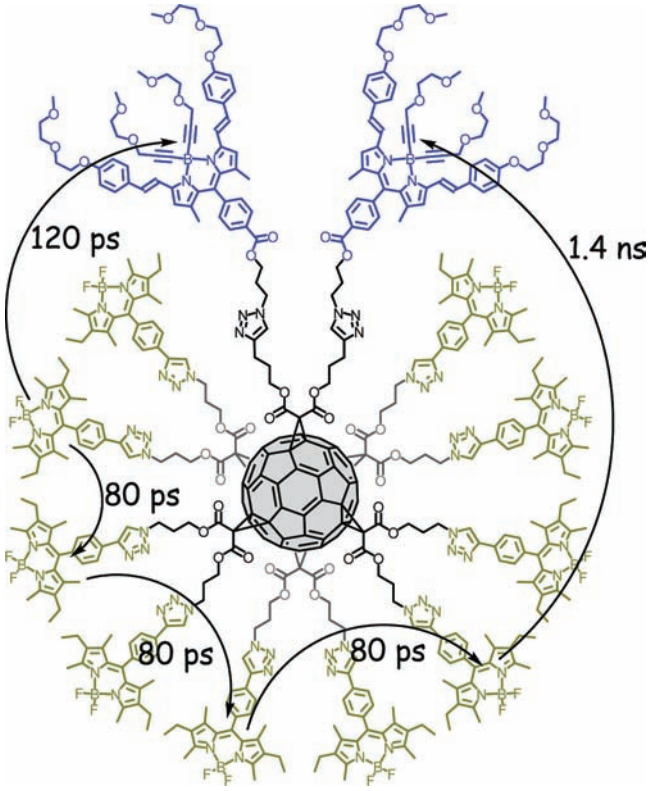

[a]The particular example shown refers to initial excitation of a dye positioned at an equatorial site and involves a random walk of the exciton in competition to trapping at a blue dye.

tether. The average center-to-center separation derived from these molecular dynamics simulations (R_{CC} = 16 ± 2 Å) is much smaller than the critical distance (R_{CD} = 23.5 Å) for energy migration between yellow dye molecules. This leads to an estimate for the average rate constant for photon hopping between yellow dyes of ca. 1.2 × 10^{10} s^{-1}. Repeating the molecular dynamics simulations with the pair of blue dyes in place indicates that, at any given time, four yellow dyes (termed proximal) reside close to a blue dye with an average center-to-center separation of 13 ± 2 Å while the B−B separation between blue dyes becomes ca. 20 Å. For these proximal yellow dyes, the average rate of EET from yellow to blue dye, based on the computed R_{CD} of 20.3 Å, is 8 × 10^9 s^{-1}. Four other yellow dyes, attached at the "equatorial" sites, are situated further from a blue dye (R_{CC} = 26 ± 5 Å) and are better positioned for energy migration to a nearby yellow dye than EET to a blue dye, because the expected average rate for the latter step is 6 × 10^8 s^{-1}. Of course, it has to be realized that the remaining two yellow dyes, appended at the "axial" position, lie far outside the region where EET to a blue dye is likely to take place, but these excited states are still able to enter into energy migration with other yellow dyes. Note that studies[33] made with simple Bodipy dyes dispersed in membranes have concluded that fluorophores residing within 13.7 Å at the moment of excitation can form an emissive dimer, but such species were not seen here.

Using the above kinetic information, it is possible to compute a further estimate of P_{EET} on the basis of statistical arguments[34] using the above kinetic guidelines. The simulation assumes

dx.doi.org/10.1021/ja206894z | J. Am. Chem.Soc. 2012, 134, 988−998

selective excitation of a yellow dye located at proximal (2000 excitations), distal (2000 excitations), or axial (1000 excitations) sites and considers the consequencies of a total of 5000 separate excitations. The calculation is made on the basis of the Bayes theorem[35] and follows the general lines used by the Monte Carlo-based ExiFRET program.[36] The net result is that the computation leads to an overall P_{EET} value of 74 ± 8%. Thus, all the various indicators are consistent with the notion of efficient trapping of the exciton by a blue dye and fast energy migration among the yellow dyes in 3D space for an isolated nanoparticle.

Electronic Energy Transfer in Plastic Films. It is now routine practice to produce spin-coated PMMA films of predetermined thickness free from serious defects.[37] Thus, spin-coated PMMA films of 1−2 μm thickness loaded with low concentrations (0.1 g/mL initial $CHCl_3$ solution) of $\mathbf{Y_{10}B_2C_{60}}$ exhibit fluorescence spectra comparable to those recorded for dioxane solutions; notably, emissions from both yellow and blue dyes are apparent. The ratio of emission bands indicates that intraparticle EET occurs with ca. 80% probability in the film. It was not possible to record meaningful fluorescence decay curves on these thin films, but this proved possible with thicker (i.e., 20 μm) films doped with low concentrations of nanoparticles. Indeed, laser excitation of a PMMA film loaded with a low density (i.e., 0.25−0.60 mg/mL of initial $CHCl_3$ solution) of $\mathbf{Y_{10}C_{60}}$ leads to nonexponential decay curves that could be analyzed in terms of eq 1 with β = 0.88 and τ_K = 1.55 ns. The derived β falls well short of that needed for monoexponential kinetics, but the mean lifetime ($\langle\tau\rangle$ = 1.62 ns) is consistent with that found in solution phase.

Under the same conditions, time-resolved emission decay profiles recorded for fluorescence from the yellow dye component of $\mathbf{Y_{10}B_2C_{60}}$ show that the lifetime is greatly reduced relative to $\mathbf{Y_{10}C_{60}}$, giving a mean lifetime $\langle\tau\rangle$ of 245 ps (Figure 7). Comparison of the two sets of data gives a P_{EET} of ca. 85% in the PMMA film. This finding indicates that, under these conditions, fluorescence quenching is a dynamic process and is not caused by self-association of yellow dyes within the polymer matrix. Analysis of the decay curves in terms of eq 1 leads to estimates of τ_K = 140 ps and β = 0.54. For the same films, fluorescence from the blue dye, following initial excitation into the yellow dye, also decays nonexponentially but on a relatively slow time scale (Figure 7). Here, nonlinear, least-squares analysis leads to $\langle\tau\rangle$ = 2.3 ns and with β = 0.93. At low densities, therefore, the nanoparticles act individually, and there is no tendency for self-association of the appended dyes in the polymer. Furthermore, the bulk of the emission observed for the blue dye grows-in after the excitation pulse, and this is taken as clear evidence for intraparticle EET along the lines indicated in Scheme 1. This growth in the emission signal is nonexponental and is difficult to analyze with meaningful precision because of the overlapping decay process.

Unlike fluid solution where the solubility of $\mathbf{Y_{10}B_2C_{60}}$ is limited to <250 μM, it is possible to load the film with relatively high densities of nanoparticles without fear of self-absorption of emitted photons. As the loading of $\mathbf{Y_{10}B_2C_{60}}$ increases so does P_{EET}, reaching a maximal value of almost 90% but starting to decrease as the loading tends toward saturation (Figure 8). This elevated efficacy can be attributed to interparticle energy transfer between neighboring nanoparticles in the film (Scheme 2). Support for this hypothesis comes from an experiment where a modest loading of $\mathbf{Y_{10}B_2C_{60}}$ (0.4 mg/mL) is augmented by the progressive addition of $\mathbf{Ph_{10}C_{60}}$. As the

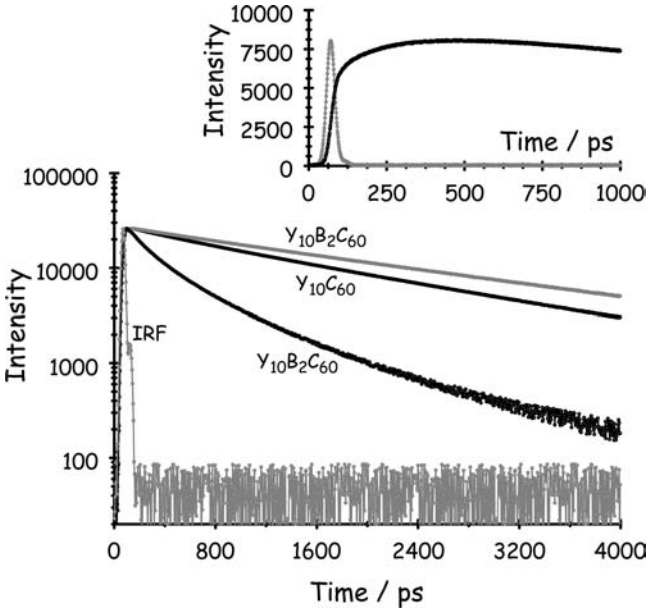

Figure 7. Time-resolved fluorescence decay curves recorded for isolated nanoparticles in PMMA. The main panel shows decay profiles for $\mathbf{Y_{10}C_{60}}$ and for yellow (lower black curve) and blue (upper gray curve) dyes associated with $\mathbf{Y_{10}B_2C_{60}}$ following direct excitation into that unit. Also shown is the IRF. The upper panel shows the decay curve recorded for the blue dye following excitation into the yellow dye for $\mathbf{Y_{10}B_2C_{60}}$ in PMMA.

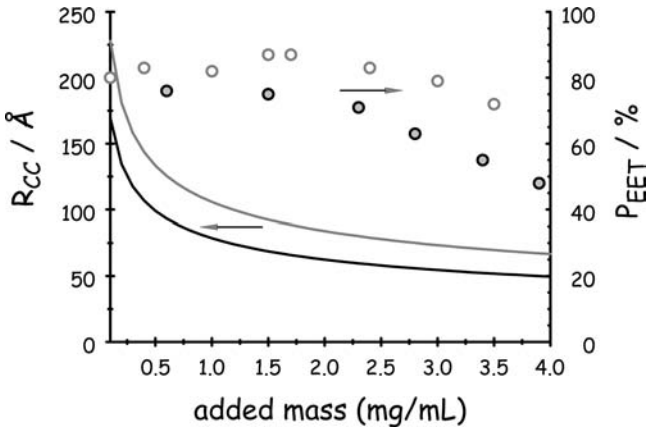

Figure 8. Effect of loading on the experimentally derived probability of EET from yellow to blue dyes when the decorated nanoparticles are dispersed in PMMA. Also shown are the center-to-center separation distances between particles as calculated from the respective density on the basis of a regular lattice. The gray curve and open gray circles refer to loading of $\mathbf{Y_{10}B_2C_{60}}$ while the black curve and filled circles refer to addition of $\mathbf{Ph_{10}C_{60}}$. In each case, the experiment starts with $\mathbf{Y_{10}B_2C_{60}}$ (0.4 mg/mL) dispersed in the film.

density of the dye-free fullerene increases, fluorescence from the blue absorber decreases, and there is a steady fall in P_{EET} (Figure 8), which can be attributed to EET to the naked fullerene core. On this basis, we might also expect energy migration between yellow dyes bound to different particles.

Before making the necessary experiment, it is prudent to consider the nature of the nanoparticles present in the PMMA film at high loading. Conventional absorption spectroscopy cannot be used to monitor these thin films, and stacking ten films together gave noisy spectra. However, multipass reflection spectroscopy using a low incidence angle[38] overcomes many of

Scheme 2. Pictorial Illustration of the Interparticle EET Steps Proposed for Selective Excitation of a Yellow Dye on a $Y_{10}C_{60}$-Decorated Nanoparticle in the Presence of Neighboring Particles[a]

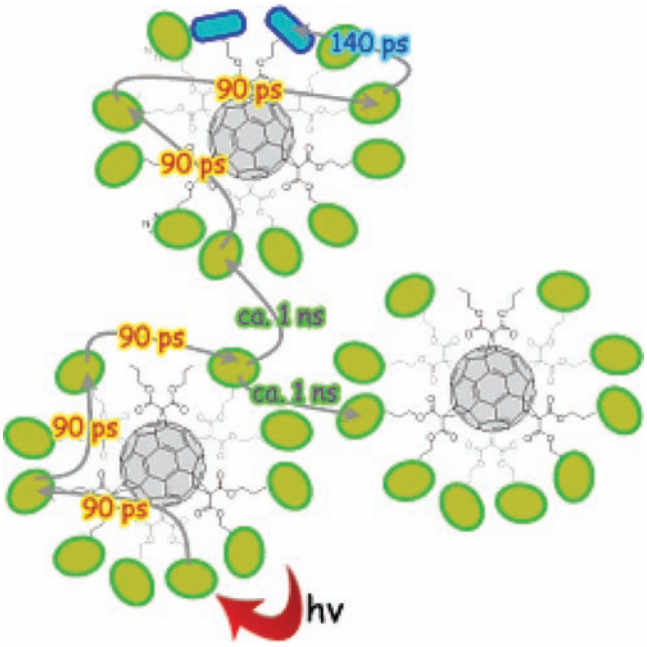

[a]It is considered that the exciton can migrate around the particle and between particles in an incoherent fashion until trapped at a blue dye.

these experimental difficulties and confirms that the dyes are present in nonaggregated forms; N.B. aggregated Bodipy dyes tend to absorb at a wavelength longer than that of the corresponding monomer and are sometimes emissive.[27] The transmission spectra recorded for thin films at ca. 8° incidence angle are essentially independent of concentration over a modest range. Aggregation becomes more likely as the solution concentration of PMMA decreases, as the solvent becomes more volatile, and as the spinning rate increases, but we were careful to control such conditions. The density of the PMMA films is 1.18 g/cm^3 while the refractive index under sodium light illumination is 1.49.[39]

The experiment set up to demonstrate interparticle EET can now be described as follows: A series of spin-coated PMMA films of 1−2 μm thickness were prepared to contain a fixed loading (2 mg/mL initial $CHCl_3$ solution) of nanoparticles. The $CHCl_3$ solution, comprising a mixture of $\mathbf{Y_{10}B_2C_{60}}$ and $\mathbf{Y_{10}C_{60}}$, was adjusted such that the mole fraction (X_B)[40] of the blue absorber was reduced gradually by dilution with $\mathbf{Y_{10}C_{60}}$. The ratio of "yellow/blue" fluorescence signals moved progressively in favor of the yellow dye with decreasing density of the blue dye but fell well short of that predicted for noncommunicating particles (i.e., no interparticle EET). Under conditions of high loading in the film, interparticle energy transfer can occur from yellow to blue dye, as already demonstrated, but also between yellow dyes (Scheme 2). The latter situation corresponds to a random walk of the exciton until trapped by EET to a blue dye. In this way, photon migration can occur over extended distances and in three dimensions; for the lowest value of X_B, where P_{EET} = 20%, the average center-to-center distance between (nonrandomly distributed!) particles is calculated as 77 Å, but the distance between nearest dye molecules will lie within the range 20−30 Å. As a consequence, trapping remains observable despite the low density of the blue dye (Figure 9). The same experiment carried out in dioxane solution simply shows an increasing proportion of emission from the yellow dye because the average interparticle separation distance (e.g., >200 Å) is too much to support long-range EET between nearest nanoparticles.

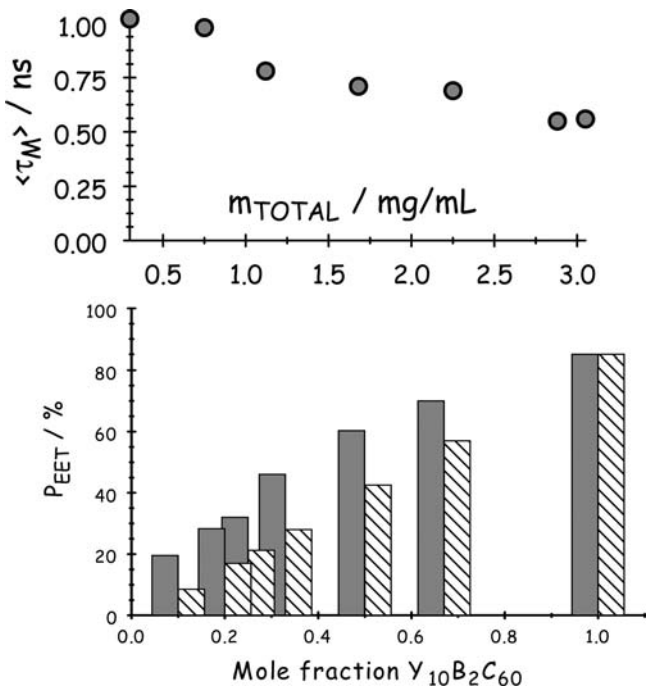

Figure 9. Lower panel: Evolution of the probability of EET from yellow to blue dyes on loading the PMMA film containing a fixed amount of $\mathbf{Y_{10}B_2C_{60}}$ with $\mathbf{Y_{10}C_{60}}$. The shaded bars refer to the experimental value while the hatched bar is the probability calculated in the absence of interparticle EET. Upper panel: Effect of total concentration of nanoparticles on the mean survival lifetime of emission from the yellow dye as measured for a 1:1 w/w mixture of $\mathbf{Y_{10}B_2C_{60}}$ and $\mathbf{Y_{10}C_{60}}$.

In a second experiment, a 1:1 (w/w) mixture of $\mathbf{Y_{10}C_{60}}$ and $\mathbf{Y_{10}B_2C_{60}}$ was prepared, and quartz slides spin-coated with PMMA (20 μm) containing various concentrations (0.2 to 2.5 mg/mL initial $CHCl_3$ solution) of this mixture were interrogated by time-resolved fluorescence spectroscopy. Illumination was restricted to the yellow dye and the mean survival time ($\langle\tau_M\rangle$) for the resultant excited state was estimated by integration of the full decay curve. The derived value decreases with increasing concentration of nanoparticles, which must be a consequence of interparticle energy migration and EET. At very low density, where interparticle EET is unlikely, the computed $\langle\tau_M\rangle$ for noncommunicating nanoparticles is 0.96 ns compared to the observed value of 1.02 ns. The latter corresponds to a crude estimate for P_{EET} of 37%. As the average distance between nanoparticles decreases, there is a concomitant fall in $\langle\tau_M\rangle$ and an increase in P_{EET} (Figure 9). At the highest concentration (i.e., 3 mg/mL), where the average center-to-center separation is likely to be around 70 Å, P_{EET} has increased to almost 65%. Under these latter conditions, therefore, interparticle EET must take place with a probability of about 50%, assuming such transfer is irreversible. Since the survival time in the absence of a blue trap is 1.6 ns, it follows

dx.doi.org/10.1021/ja206894z | J. Am. Chem.Soc. 2012, 134, 988−998

that the net interparticle transfer time must be comparable at this separation distance.

Sensitization Studies. A luminescent solar concentrator (LSC) is a thin, flat plate of highly fluorescent material that directs most of the emission to its edges by way of total internal reflection; the probability of a photon absorbed in the bulk plastic resulting in emission of a photon at the edge can reach as high as 75%. A solar cell, attached to the edges with an index matching material and selected such that its band gap blends with the fluorescence profile, can utilize this emission for electricity generation. A complementary device, for example, might use the LSC to activate a photosensor for control of street lighting. Numerous types of fluorescent materials have been proposed for use in LSCs, including organic dyes,[41] inorganic phosphors,[42] and quantum dots,[43] although single compounds tend not to absorb a viable fraction of the solar spectrum or are poorly matched to the photovoltaic substrate. The most serious drawback of commercial LSCs, apart from limited photostability, relates to self-absorption of the fluorescence. Mixtures of dyes have been used[44] to overcome the light-collection problem, and the possibility of intermolecular EET has been considered[45] as a means to reduce self-absorption. It might be considered in this respect that the decorated nanoparticles investigated here represent superior prototypes for LSCs, and this concept will be fully explored in future work.

As a crude test of the basic concept, a flat-plate, single-layer PMMA-based LSC was cast to contain a low density of $\mathbf{Y_{10}B_2C_{60}}$ (0.5 mg/mL) and used to sensitize an amorphous silicon photocell. The action spectrum for this photovoltaic cell (open circuit voltage of 0.85 V), with its onset at 750 nm, overlaps nicely with emission from the yellow and blue dyes while the optical spectrum of $\mathbf{Y_{10}B_2C_{60}}$ does not promote self-absorption. The flexible photocell, which was found to operate with an average light-to-electricity conversion efficiency of ca. 5% under ambient light conditions, was coated with a single layer of antireflective Ta_2O_5, which is effective for the 550 to 700 nm region. The photocell was glued to the edge of the LSC (width 3 mm and surface area 25 cm^2). On exposure of the LSC in a solar simulator matching the AM 1.5 spectrum, the current from the photocell was found to increase linearly with increasing light intensity over 2 orders of magnitude. Under illumination at 510 ± 15 nm, where the yellow Bodipy dye is the primary light absorber, the LSC gave a 3.2-fold increase in current[46] relative to direct illumination of the photocell cut to the same surface area (4.5 cm^2) as used with the LSC. Long-term exposure to sunlight resulted in partial decomposition of the blue dye but not the yellow dye. Nonetheless, this should be considered as a successful proof-of-concept for the fabrication of next-generation LSCs.

CONCLUDING REMARKS

Once again, we are faced with the urgent need to develop viable strategies for providing energy from renewable sources. The most attractive, and for many scientists, the most promising approach to this aim involves solar fuel production by way of bioinspired artificial photosynthesis. In this respect, it is important to note that the natural photosynthetic apparatus uses an elaborate light-harvesting array[2,47] to collect incident sunlight and channel the resultant excitons to a site where fuel generation can take place.[48] The light harvester plays several crucial roles but has been largely overlooked in the race to develop artificial photosystems based on light-induced electron transfer. The photon collector described herein involves accretion of fluorescent dyes around a fullerene core; a major synthetic challenge that now provides access to a wide range of tailored emitters with novel properties. The current prototype, although far from optimized, increases the performance of amorphous Si solar cells by providing a much enhanced absorption profile that is not subjected to problems from self-absorption.

The main attribute of the new system is that it closely mimics the most important features of the natural array.[2,47] It operates in the solid state, it is based on a principle of energy migration around and between clusters decorated with identical chromophores, and it facilitates large-scale energy transport to a trap. The mechanism and rates of both intra- and interparticle energy transfers have been exposed by way of emission spectroscopy. The overall efficacy falls progressively with decreasing mole fraction of the photon trap but remains within practical limits. The result is that photons incident over a relatively large area can be concentrated to a small trap that can initiate electron-transfer chemistry. We consider this prototype as being a major breakthrough in the search for artificial light-harvesting arrays. Suitable modifications can be made that should lead to photon collectors for solar cells[49] and related devices such as ambient light photosensors.

This artificial light-harvesting array reproduces many of the essential features of its natural analogue,[1,2] albeit at slower rates over shorter distances and with lower overall efficacy. Nonetheless, we can anticipate important improvements in performance with next-generation prototypes, especially since there are several key synthetic variables open to exploitation. Increasing the rates of energy transfer and migration is possible simply by changing the nature of the dyes used to decorate the C_{60} surface and the type of linker but without losing the flexibility of the so-called "click" couplage. Minimizing photon loss due to competitive energy transfer to the C_{60} core can be treated in terms of the spectral overlap integral and managed accordingly. The biggest challenge lies with self-assembling the loaded C_{60} particles into a loose network where interparticle energy transfer is highly favored.

ASSOCIATED CONTENT

Supporting Information

Synthesis and characterization of new compounds, details of calculations for light-induced electron transfer and Förster critical distances, and average conformations on the nanoparticles. This material is available free of charge via the Internet at http://pubs.acs.org.

AUTHOR INFORMATION

Corresponding Author

harriman@ncl.ac.uk; nierengarten@unistrasbg.fr; ziessel@unistra.fr

ACKNOWLEDGMENTS

We thank the CNRS, EPSRC, Newcastle University, and ECPM - Strasbourg for their financial support of this work. We thank Dr. Ruth Ryan for preparing the thin films.

REFERENCES

(1) Cheng, Y. C.; Fleming, G. R. *Annu. Rev. Phys. Chem.* **2009**, *60*, 241−262.

(2) (a) McDermott, G.; Prince, S. M.; Freer, A. A.; Hawthornthwaite-Lawless, A. M.; Papiz, M. Z.; Cogdell, R. J.; Isaacs, N. W. *Nature* **1995**,

374, 517−521. (b) Hawthornthwaite, A. M.; Cogdell, R. J. In *The Chlorophylls*; Scheer, H., Ed.; CRC Press, Boca Raton, 1993; pp 493−528. (c) Karrasch, S.; Bullough, P. A.; Ghosh, R. *EMBO J.* **1995**, *14*, 631−638.
(3) (a) Blankenship, R. E. *Molecular Mechanisms of Photosynthesis*; Blackwell Science: Oxford, 2002. (b) van Amerongen, H.; Valkunas, L.; van Grondelle, R. *Photosynthetic Excitons*; World Scientific: Singapore, 2000.
(4) Engel, G. S.; Calhoun, T. R.; Read, E. L.; Ahn, T. K.; Mancal, T.; Cheng, Y. C.; Blankenship, R. E.; Fleming, G. R. *Nature* **2007**, *446*, 782−786.
(5) (a) Choi, M. S.; Yamazaki, T.; Yamazaki, I.; Aida, T. *Angew. Chem., Int. Ed.* **2004**, *43*, 150.158. (b) Adronov, A.; Gilat, S. L.; Frechet, J. M. J.; Ohta, K.; Neuwahl, F. V. R.; Fleming, G. R. *J. Am. Chem. Soc.* **2000**, *122*, 1175−1185. (c) Yeow, E. K. L.; Ghiggino, K. P.; Reek, J. N. H.; Crossley, M. J.; Bosman, A. W.; Schenning, A. P. H. J.; Meijer, E. W. *J. Phys. Chem. B* **2000**, *104*, 2596−2606.
(6) (a) Holden, D. A.; Guillet, J. E. *Macromolecules* **1980**, *13*, 289−295. (b) Collini, E.; Scholes, G. D. *Science* **2009**, *323*, 369−373. (c) Webber, S. E. *Chem. Rev.* **1990**, *90*, 1469−1482.
(7) (a) George, S. J.; Ajayaghosh, A. *Chem.—Eur. J.* **2005**, *11*, 3217−3227. (b) Ajayaghosh, A.; Praveen, V. K.; Vijayakumar, C. *Chem. Soc. Rev.* **2008**, *37*, 109−122.
(8) Scholes, G. D.; Rumbles, G. *Nat. Mater.* **2006**, *5*, 683−696.
(9) Barnham, K. W. J.; Marques, J. L.; Hassard, J.; O'Brien, P. *Appl. Phys. Lett.* **2000**, *76*, 1197−1201.
(10) Hirsch, A.; Vostrowsky, O. *Eur. J. Org. Chem.* **2001**, 829−848.
(11) (a) Iehl, J.; Nierengarten, J.-F. *Chem.—Eur. J.* **2009**, *15*, 7306−7309. (b) Nierengarten, J.-F.; Iehl, J.; Oerthel, V.; Holler, M.; Illescas, B. M.; Munoz, A.; Martin, N.; Rojo, J.; Sanchez-Navarro, M.; Cecioni, S.; Vidal, S.; Buffet, K.; Durka, M.; Vincent, S. P. *Chem. Commun.* **2010**, *46*, 3860−3862. (c) Iehl, J.; Nierengarten, J.-F. *Chem. Commun.* **2010**, *46*, 4160−4162.
(12) (a) Diekers, M.; Luo, C.; Guldi, D. M.; Hirsch, A. *Chem.—Eur. J.* **2002**, *8*, 979−991. (b) Iehl, J.; Holler, M.; Nierengarten, J.-F.; Yoosaf, K.; Malicka, J. M.; Armaroli, N.; Strub, J.-M.; Van Dorsselaer, A.; Delavaux-Nicot, B. *Aust. J. Chem.* **2011**, *64*, 153−159.
(13) (a) Cardullo, F.; Seiler, P.; Isaacs, L.; Nierengarten, J.-F.; Haldimann, R. F.; Diederich, F.; Mordasini-Denti, T.; Thiel, W.; Boudon, C.; Gisselbrecht, J.-P.; Gross, M. *Helv. Chim. Acta* **1997**, *80*, 343−371. (b) Camps, X.; Dietel, E.; Hirsch, A.; Pyo, S.; Echegoyen, L.; Hackbarth, S.; Röder, B. *Chem.—Eur. J.* **1999**, *5*, 2362−2373. (c) Iehl, J.; Pereira de Freitas, R.; Delavaux-Nicot, B.; Nierengarten, J.-F. *Chem. Commun.* **2008**, 2450−2452.
(14) (a) Lammi, R. K.; Wagner, R. W.; Ambroise, A.; Diers, J. R.; Bocian, D. F.; Holten, D.; Lindsey, J. S. *J. Phys. Chem. B* **2001**, *105*, 5341−5352. (b) Holten, D.; Bocian, D. F.; Lindsey, J. S. *Acc. Chem. Res.* **2002**, *35*, 57−69.
(15) (a) Ziessel, R.; Harriman, A. *Chem. Commun.* **2011**, *47*, 611−631. (b) Ziessel, R.; Allen, B. D.; Rewinska, D. B.; Harriman, A. *Chem.—Eur. J.* **2009**, *27*, 7382−7393. (c) Wijesinghe, C. A.; El-Khouly, M. E.; Blakemore, J. D.; Znadler, M. E.; Fukuzumi, S.; D'Souza, F. *Chem. Commun.* **2010**, *46*, 3301−3303. (d) Liu, J. Y.; El-Khouly, M. E.; Fukuzumi, S.; Ng, D. K. *Chem. Asian J.* **2011**, *3*, 174−179.
(16) (a) Ranca, F.; Helmreich, M.; Mölich, A.; Hermilov, E. A.; Jux, N.; Röder, B.; Hirsch, A.; Böhm, F. *Bioconjugate Chem.* **2007**, *18*, 1078−1086. (b) Regehly, M.; Hermilov, E. A.; Mölich, A.; Helmreich, M.; Hirsch, A.; Jux, N.; Röder, B. *J. Phys. Chem. B* **2007**, *111*, 998−1006.
(17) (a) Herzog, A.; Hirsch, A.; Vostrowsky, O. *Eur. J. Org. Chem.* **2000**, 171−180. (b) Iehl, J.; Nierengarten, J.-F. *Chem. Commun.* **2010**, *46*, 4160−4162. (c) Fortgang, P.; Maisonhaute, E.; Amatore, C.; Delavaux-Nicot, B.; Iehl, J.; Nierengarten, J.-F. *Angew. Chem., Int. Ed.* **2011**, *50*, 2364−2367.
(18) (a) Ulrich, G.; Ziessel, R. *J. Org. Chem.* **2004**, *69*, 2070−2083. (b) Ziessel, R.; Bonardi, L.; Retailleau, P.; Ulrich, G. *J. Org. Chem.* **2006**, *71*, 3093−3096. (c) Benniston, A. C.; Copley, G.; Elliott, K. J.; Harrington, R. W.; Clegg, W. *Eur. J. Org. Chem.* **2008**, 2705−2713. (d) Hisato, S.; Yasuteru, U.; Hirotatsu, K.; Tetsuo, N. *J. Am. Chem. Soc.* **2007**, *129*, 5597−5604.
(19) (a) Rousseau, T.; Cravino, A.; Roncali, J.; Bura, T.; Ulrich, G.; Ziessel, R. *Chem. Commun.* **2009**, 1673−1675. (b) Rousseau, T.; Cravino, A.; Roncali, J.; Bura, T.; Ulrich, G.; Ziessel, R. *J. Mater. Chem.* **2009**, *16*, 2298−2300. (c) Rousseau, T.; Cravino, A.; Ripaud, E.; Leriche, P.; Rihn, S.; De Nicola, A.; Ziessel, R.; Roncali, J. *Chem. Commun.* **2010**, *46*, 5082−5084.
(20) (a) Kollmannsberger, M.; Rurack, K.; Resch-Genger, U.; Daub, J. *J. Phys Chem. A* **1998**, *102*, 10211−10220. (b) Burghart, A.; Kim., H.; Wech, M. B.; Thorensen, L. H.; Reibenspies, J.; Burgess, K. *J. Org. Chem.* **1999**, *64*, 7813−7819. (c) Wan, C.-W.; Burghart, A.; Chen, J.; Bergström, F.; Johanson, L. B.-A.; Wolford, M. F.; Kim, T. G.; Topp, M. R.; Hochstrasser, R. M.; Burgess, K. *Chem.—Eur. J.* **2003**, *9*, 4430−4441. (d) Bricks, J. L.; Kovalchuk, A.; Trieflinger, C.; Nofz, M.; Büschel, M.; Tolmachev, A. I.; Daub, J.; Rurack, K. *J. Am. Chem. Soc.* **2005**, *127*, 13522−13529. (e) Cotlet, M.; Vosch, T.; Habichi, S.; Weil, T.; Müllen, K.; Hofkens, J.; De Schryver, F. *J. Am. Chem. Soc.* **2005**, *127*, 9760−9768.
(21) (a) Kumaresan, D.; Thummel, R. P.; Bura, T.; Ulrich, G.; Ziessel, R. *Chem.—Eur. J.* **2009**, *15*, 6335−6339. (b) Ziessel, R.; Ulrich, G.; Olivier, J. H.; Bura, T.; Sutter, A. *Chem. Commun.* **2010**, *46*, 7978−7980.
(22) Renger, T. *Photosynth. Res.* **2009**, *102*, 471−485.
(23) Wong, K. F.; Bagchi, B.; Rossky, P. J. *J. Phys. Chem. A* **2004**, *108*, 5752−5763.
(24) (a) Guldi, D.; Hauke, F.; Hirsch, A. *Res. Chem. Intermed.* **2002**, *28*, 817−830. (b) The photophysical properties recorded for $Ph_{10}C_{60}$ in toluene are: $\Phi_F = 7 \times 10^{-4}$, $\tau_S = 1.65$ ns, $E_S = 1.87$ eV.
(25) Ying, Q.; Marecek, J.; Chu, B. *Chem. Phys. Lett.* **1994**, *219*, 214−218.
(26) (a) Guldi, D. M. *Chem. Soc. Rev.* **2002**, *31*, 22−36. (b) Kuciauskas, D.; Lin, S.; Seely, G. R.; Moore, A. L.; Moore, T. A.; Gust, D.; Drovetskaya, T.; Reed, C. A.; Boyd, P. D. W. *J. Phys. Chem.* **1996**, *100*, 15926−15932. (c) Kodis, G.; Liddell, P. A.; de la Garza, L.; Clausen, P. C.; Lindsey, J. S.; Moore, A. L.; Moore, T. A.; Gust, D. *J. Phys. Chem. A* **2002**, *106*, 2036−2048. (d) Allen, B. D.; Benniston, A. C.; Harriman, A.; Mallon, L. J.; Pariani, C. *Phys. Chem. Chem. Phys.* **2006**, *8*, 4112−4118. (e) Ziessel, R.; Allen, B. D.; Rewinska, D. B.; Harriman, A. *Chem.—Eur. J.* **2009**, *15*, 7382. (f) Guldi, D. M.; Luo, C. P.; Prato, M.; Troisi, A.; Zerbetto, F.; Scheloske, M.; Dietel, E.; Bauer, W.; Hirsch, A. *J. Am. Chem. Soc.* **2001**, *123*, 9166−9167.
(27) (a) Tokoro, Y.; Nagai, A.; Chujo, T. *Tetrahedron Lett.* **2010**, *51*, 3451−3454. (b) Bergstrom, F.; Mikhalyov, I.; Hagglof, P.; Wortmann, R.; Ny, T.; Johansson, L. B.-Å. *J. Am. Chem. Soc.* **2002**, *124*, 196−204. (c) Tleugabulova, D.; Zhang, Z.; Brennan, J. D. *J. Phys. Chem. B* **2002**, *106*, 13133−13138. (d) Benniston, A. C.; Copley, G.; Harriman, A.; Howgego, D.; Harrington, R. W.; Clegg, W. *J. Org. Chem.* **2010**, *75*, 2018−2027. (e) Harriman, A.; Mallon, L. J.; Stewart, B.; Ulrich, G.; Ziessel, R. *Eur. J. Org. Chem.* **2007**, 3191−3198.
(28) (a) Benny Lee, K. C.; Siegel, J.; Webb, S. E. D.; Lévêque-Fort, S.; Cole, M. J.; Jones, R.; Dowling, K.; Lever, M. J.; French, P. M. W. *Biophys. J.* **2001**, *81*, 1265−1274. (b) Tcherkasskaya, O.; Spiro, J. G.; Ni, S. R.; Winnik, M. A. *J. Phys. Chem.* **1996**, *100*, 714−721. (c) Duportail, G.; Merola, F.; Llanos, P. *J. Photochem. Photobiol., A* **1995**, *89*, 135−140. (d) Van der Auweraer, M.; Ballet, P.; De Schryver, F. C.; Kowalczyk, A. *Chem. Phys.* **1994**, *187*, 399−416.
(29) Berberan-Santos, M. N.; Bodunov, E. N.; Valeur, B. *Chem. Phys.* **2005**, *315*, 171−182.
(30) Förster, T. *Ann. Phys. (Leipzig)* **1948**, *2*, 55−75.
(31) Deplazes, E.; Jayatilaka, D.; Corry, B. *Phys. Chem. Chem. Phys.* **2011**, *13*, 11045−11054.
(32) Schönberger, H.; Schwab, C. H.; Hirsch, A.; Gasteiger, J. *J. Mol. Model.* **2000**, *6*, 379−395.
(33) Dahim, M.; Mizuno, N. K.; Li, X. M.; Momsen, W. E.; Momsen, M. M.; Brockman, H. L. *Biophys. J.* **2002**, *83*, 1511−1524.
(34) (a) Klafter, J.; Blumen, A. *J. Chem. Phys.* **1984**, *80*, 875−877. (b) Zumofen, G.; Blumen, A. *Chem. Phys. Lett.* **1982**, *88*, 63−67.

(35) Jaynes, E. T. *Probability Theory: The Logic of Science*; Cambridge University Press: Cambridge, UK, 2003.
(36) Corry, B.; Jayatilaka, D.; Rigby, P. *Biophys. J.* **2005**, *89*, 3822−3836.
(37) Walsh, C. B.; Franses, E. I. *Thin Solid Films* **2003**, *429*, 71−76.
(38) Holzer, W.; Pichlmaier, M.; Drotleff, E.; Penzkofer, A.; Bradley, D. D. C.; Blau, W. J. *Opt. Commun.* **1999**, *163*, 24−28.
(39) Paudler, M.; Ruths, J.; Rieger, H. *Langmuir* **1992**, *8*, 184−189.
(40) The mole fraction refers exclusively to the decorated C_{60} particles, excluding PMMA and solvent, and considers the entire particle rather than the appended dye.
(41) (a) Hermann, A. M. *Sol. Energy* **1982**, *29*, 323−328. (b) Reisfeld, R.; Joergensen, C. K. *Struct. Bonding (Berlin, Ger.)* **1982**, *49*, 1−14.
(42) Popov, V. V.; Yakimenko, V. N. *J. Appl. Spectrosc.* **1995**, *62*, 573−578.
(43) (a) Chatten, A. J.; Barnham, K. W. J.; Buxton, B. F.; Ekins-Daukes, N. J.; Malik, M. A. *Sol. Energy Mater. Sol. Cells* **2003**, *75*, 363−369. (b) Chatten, A. J.; Barnham, K. W. J.; Buxton, B. F.; Ekins-Daukes, N. J.; Malik, M. A. *Semiconductors* **2004**, *38*, 909−915.
(44) Swartz, B. A.; Cole, T.; Zewail, A. H. *Opt. Lett.* **1977**, *1*, 73−77. (b) Batchelder, J. S.; Zewail, A. H.; Cole, T. *Appl. Opt.* **1981**, *20*, 3733.
(45) Bailey, S. T.; Lokey, G. E.; Hanes, M. S.; Shearer, J. D. M.; McLafferty, J. B.; Beaumont, G. T.; Baseler, T. T.; Layhue, J. M.; Broussard, D. R.; Zhang, Y.-Z.; Wittmershaus, B. P. *Sol. Energy Mater. Sol. Cells* **2007**, *91*, 67−75.
(46) The current increased from 14 μA to 44 μA when the plastic solar concentrator is in place.
(47) Kuhlbrandt, W.; Wang, D. N.; Fujiyoshi, Y. *Nature* **1994**, *367*, 614−621.
(48) Benniston, A. C.; Harriman, A. *Mater. Today* **2008**, *11*, 26−34.
(49) Goldschmidt, J. C.; Peters, M.; Bösch, A.; Helmers, H.; Dimroth, F.; Glunz, S. W.; Willeke, G. *Sol. Energy Mater. Sol. Cells* **2009**, *93*, 176−182.